

Asteroseismic Investigation of 20 Planet and Planet-Candidate Host Stars

C. Kayhan[★], M. Yıldız and Z. Çelik Orhan

Department of Astronomy and Space Sciences, Science Faculty, Ege University, 35100 Bornova, İzmir, Turkey

Accepted XXX. Received YYY; in original form ZZZ

ABSTRACT

Planets and planet candidates are subjected to great investigation in recent years. In this study, we analyse 20 planet and planet-candidate host stars at different evolutionary phases. We construct stellar interior models of the host stars with the MESA evolution code and obtain their fundamental parameters under influence of observational asteroseismic and non-asteroseismic constraints. Model mass range of the host stars is 0.74-1.55 M_{\odot} . The mean value of the so-called large separation between oscillation frequencies and its variation about the minima show the diagnostic potential of asteroseismic properties. Comparison of variations of model and observed large separations versus the oscillation frequencies leads to inference of fundamental parameters of the host stars. Using these parameters, we revise orbital and fundamental parameters of 34 planets and four planet candidates. According to our findings, radius range of the planets is 0.35-16.50 R_{\oplus} . The maximum difference between the transit and revised radii occurs for Kepler-444b-f is about 25 per cent.

Key words: asteroseismology – planets and satellites: fundamental parameters – stars: evolution – stars: fundamental parameters – stars: oscillations – planetary systems.

1 INTRODUCTION

Planetary studies collect huge data nowadays. Thanks to the *Convection, Rotation and planetary Transits (CoRoT*; Baglin et al. 2006), *Kepler* (Koch et al. 2010), ground-base observations and *Transiting Exoplanet Survey Satellite (TESS*; Sullivan et al. 2015), more than 3900¹ planets are discovered. Fate of a planet is determined and characterized by its host star. Accuracy of the fundamental planetary parameters depends on how exact properties of the host stars we compute. Most of the observed planet and planet candidate host stars have convective envelope. Thus, they exhibit solar-like oscillations. Long-period observations with high precise data allow to reveal solar-like oscillation frequencies. Hereby, fundamental parameters of host stars are derived from asteroseismic methods with the reference frequencies (Yıldız et al. 2014, hereafter Paper I; Yıldız, Çelik Orhan & Kayhan 2015, hereafter Paper II) and scaling relations (see e.g. Mathur et al. 2012; Huber et al. 2013).

From *CoRoT* and *Kepler* observations, many solar-like oscillating host stars have been discovered. First remarkable

studies that derive stellar parameters of the host stars in great number using asteroseismology are for *Kepler* planet-candidate host stars (Huber et al. 2013; Silva Aguirre et al. 2015). Before *Kepler*, some studies that are based on *CoRoT*, *Hubble* and ground-based observations are seen in the literature (see e.g. Soriano et al. 2007; Nutzman et al. 2011; Wright et al. 2011). In this study, we construct interior models of 20 *Kepler* and *CoRoT* target host stars with the MESA stellar evolution code (Paxton et al. 2011, 2013). We compute adiabatic oscillation frequencies of the models and compare them with observed oscillation frequencies with ADIPLS package and try to obtain fundamental parameters of the host stars and their planets.

Since large separation between oscillation frequencies ($\Delta\nu$) is related to sound travel time throughout stellar radius (R), mean stellar density derived from asteroseismology is more accurate than the mean density derived from any method (Ulrich 1986). If effective temperature (T_{eff}) is observed precisely, R and stellar mass (M) are determined using the asteroseismic quantities, namely, frequency of the maximum amplitude (ν_{max}), $\Delta\nu$ and reference frequencies ($\nu_{\text{min}0}$, $\nu_{\text{min}1}$, and $\nu_{\text{min}2}$; Paper I and II) at the minima of $\Delta\nu$, in conventional (Kjeldsen & Bedding 1995) and new scaling relations (Yıldız, Çelik Orhan & Kayhan 2016, hereafter Paper III). Stellar age is derived from stellar interior

[★] E-mail: cenkkayhan@gmail.com

¹ <http://exoplanetarchive.ipac.caltech.edu/>

models. As hydrogen fused into helium in the nuclear core, mean molecular weight increases and sound speed gradient changes in time. Therefore, the small separation between oscillation frequencies ($\delta\nu_{02}$) is much more sensitive function of the nuclear processes in the core than individual oscillation frequencies. Hence, age of main-sequence (MS) stars determined by $\delta\nu_{02}$ is much more precise than ages from any method (Ulrich 1986).

Most of the planets is discovered by observing their transit across the disk of the hosts (see e.g. Steffen et al. 2012; Rowe et al. 2014). Planets have also been detected by radial velocity (RV) method. Although mass of a planet directly estimated from the RV method depends on inclination of its orbit (see e.g. Borucki et al. 2010; ?; Barclay et al. 2015), for both methods, properties of the host stars are required for determination of the fundamental planetary parameters. In this study, we construct interior models for the host stars and obtain their parameters under asteroseismic and non-asteroseismic constraints. Then, we revise fundamental and orbital parameters of 34 planets and four planet-candidates using model mass and radius of the host stars (see Section 4).

We organize this paper as follows. In Section 2, we give basic properties of the host stars inferred from asteroseismic and non-asteroseismic observational data. MESA models and seismic analysis of the host stars are presented in Section 3. In Section 4, we estimate fundamental and orbital parameters of the planets and planet candidates. Lastly, we draw our conclusions in Section 5.

2 ASTEROSEISMIC AND NON-ASTEROSEISMIC PROPERTIES OF THE HOST STARS

The host stars have different evolutionary phases. They exhibit solar-like oscillations. Thus, we have opportunity to analyse the host stars with asteroseismology. Observed asteroseismic and spectral properties of the host stars are listed in Table 1. Among the host stars, HD 52265 is the only star observed by *CoRoT*. The remaining stars are observed by *Kepler*. Observational oscillation frequencies of the host stars that are obtained from *CoRoT* and *Kepler* light curves are taken from the literature (see Table 1). From observational oscillation frequencies, we obtain mean small separation between oscillation frequencies ($\langle\delta\nu_{02}\rangle$). $\Delta\nu$ and ν_{\max} are taken from the literature. $\Delta\nu$ from the literature is in very good agreement with $\Delta\nu$ obtained from $\Delta\nu$ versus ν graph. Also, we determine the reference frequencies from their $\Delta\nu$ versus ν graph. For all of the target stars, we have determined $\nu_{\min 0}$ and $\nu_{\min 1}$ from their $\Delta\nu$ versus ν graph, except KIC 10963065. For KIC 10963065, $\nu_{\min 0}$ is not available. $\nu_{\min 2}$ is partly or entirely seen in the five target stars (KIC 3632418, KIC 8866102, KIC 9592705, KIC 10666592, and KIC 11807274).

To compute ν_{\min} of any minima from $\Delta\nu$ versus ν graph, we first determine frequency interval of the minimum and draw two straight lines from the neighbourhood intervals. The intersection of the two lines corresponds ν_{\min} .

Evolutionary phases of the host stars are seen in Fig. 1. In this figure, $\Delta\nu_{\text{obs}}$ of the host stars are plotted with respect to effective temperature based on spectra ($T_{\text{eff,S}}$). Thin and

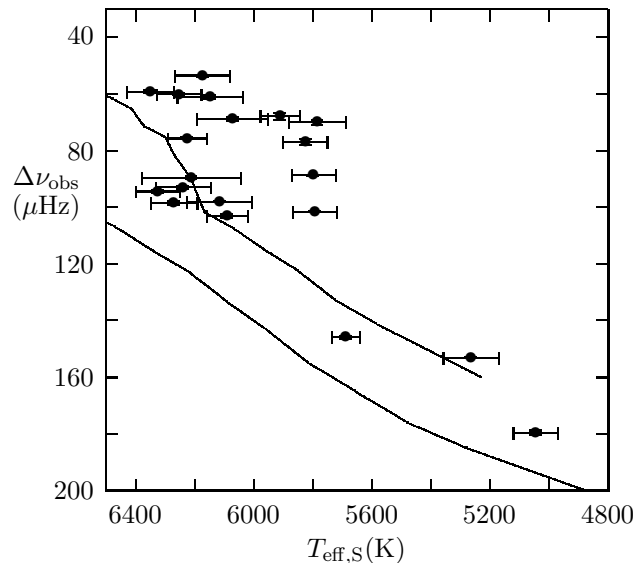


Figure 1. Large separation between observed oscillation frequencies with respect to spectroscopic effective temperature for the 20 host stars. Thin and thick solid lines are for zero-age main sequence (ZAMS) and terminal-age main sequence (TAMS), respectively.

thick solid lines are zero-age main sequence (ZAMS) and terminal-age main sequence (TAMS), respectively. These lines are computed with the MESA evolution code for the mass range $0.8-1.6 M_{\odot}$ with solar composition. Five host stars are MS star. Most of the host stars are on the sub-giant evolutionary phase. The effective temperature range of the host stars is about 5000–6350 K. KIC 10666592 is the hottest host star and its effective temperature is 6350 ± 80 K. In contrast, effective temperature of the coolest host star (KIC 6278762) is 5046 ± 74 K.

Most of the 38 planets are small rocky planets. The remaining planets are mostly hot giant. Number of multiple systems is 10. The planet with the longest period is Kepler-126c, approximately 100 d. Kepler-65c is the planet with the shortest orbital period of 2 d.

3 INTERIOR MODELS OF THE HOST STARS

3.1 Properties of the MESA code

We construct interior models of 20 host stars with MESA evolution code (Paxton et al. 2011, 2013). Standard mixing length theory (Böhm-Vitense 1958) is used for convection treatment. The effects of convective overshooting are not considered. OPAL opacity tables are taken from Iglesias & Rogers (1993, 1996). In nuclear reaction rates, we use Angulo et al. (1999) with updated by Kunz et al. (2002) and Cyburt et al. (2010). Stellar atmospheric conditions are vital for asteroseismic modelling in particular for high-frequency domain. For simplicity, we select the `SIMPLE_PHOTOSPHERE` option in MESA for the host stars (see details in Paxton et al. 2011). Element diffusion is included with MESA default option. Diffusion is taken into account for the host stars with $M_{\text{star}} < 1.2 M_{\odot}$. For the solar values, initial hydrogen abundance $X = 0.70358$, metallicity

Table 1. Observed spectral and asteroseismic properties of the host stars. Columns are organized as star name, effective temperature, surface metallicity, spectral and asteroseismic gravities, frequency of maximum amplitude, mean large and small separations between oscillation frequencies, reference frequencies for min0, min1 and min2 and references. Effective temperature and observed metallicity are taken from spectral observations. Asteroseismic gravity is computed from asteroseismic scaling relation. $\langle\delta\nu_{02}\rangle$, $\nu_{\min 0}$, $\nu_{\min 1}$, and $\nu_{\min 2}$ are derived from observed oscillation frequencies. ν_{\max} and $\Delta\nu$ are taken from the references given in the last column.

Star	$T_{\text{eff,S}}$ (K)	$[M/H]_{\text{obs}}$ (dex)	$\log g_s$ (cgs)	$\log g_{\text{sca}}$ (cgs)	ν_{\max} (μHz)	$\langle\Delta\nu\rangle$ (μHz)	$\langle\delta\nu_{02}\rangle$ (μHz)	$\nu_{\min 0}$ (μHz)	$\nu_{\min 1}$ (μHz)	$\nu_{\min 2}$ (μHz)	Ref.
HD 52265	6116 ± 110	0.22 ± 0.05	4.32 ± 0.20	4.28 ± 0.01	2090.0 ± 20	98.1 ± 0.1	8.2 ± 0.9	2338.1	1845.7	–	3,12,17
KIC 3544595	5689 ± 48	-0.15 ± 0.40	4.56 ± 0.06	4.46 ± 0.02	3366.0 ± 81	145.8 ± 0.5	8.6 ± 1.7	3283.2	2701.9	–	2,14,23
KIC 3632418	6148 ± 111	-0.19 ± 0.21	3.94 ± 0.21	4.01 ± 0.04	1159.0 ± 44	60.9 ± 0.6	4.3 ± 0.7	1422.1	1065.2	736.0	1,9,19,20
KIC 4349452	6270 ± 79	-0.04 ± 0.10	4.28 ± 0.03	4.29 ± 0.02	2106.0 ± 50	98.3 ± 0.6	7.8 ± 1.6	2365.2	1884.5	–	4,14,18
KIC 5866724	6211 ± 167	0.17 ± 0.06	4.23 ± 0.01	4.24 ± 0.03	1880.0 ± 60	89.6 ± 0.5	7.6 ± 1.2	2261.4	1698.3	–	8,14
KIC 6278762	5046 ± 74	-0.55 ± 0.07	4.60 ± 0.06	4.58 ± 0.03	4538.0 ± 144	179.6 ± 0.8	9.5 ± 1.0	4220.8	3411.7	–	6,10
KIC 6521045	5825 ± 75	0.02 ± 0.10	4.13 ± 0.03	4.13 ± 0.02	1502.0 ± 31	77.0 ± 1.1	5.3 ± 0.5	1643.2	1259.1	–	10,18
KIC 7296438	5798 ± 75	0.30 ± 0.10	4.15 ± 0.15	4.22 ± 0.01	1848.0 ± 16	88.7 ± 0.1	5.3 ± 0.3	1983.2	1540.8	–	11,13
KIC 8077137	6072 ± 121	-0.09 ± 0.15	4.07 ± 0.03	4.09 ± 0.03	1324.0 ± 39	68.8 ± 0.6	5.6 ± 1.0	1494.3	1140.0	–	10,15
KIC 8292840	6239 ± 94	-0.14 ± 0.10	4.25 ± 0.04	4.27 ± 0.02	1983.0 ± 37	92.9 ± 0.4	7.8 ± 1.3	2245.6	1730.6	–	10,22
KIC 8866102	6325 ± 75	0.01 ± 0.10	–	4.28 ± 0.02	2014.0 ± 32	94.5 ± 0.6	8.0 ± 1.7	2420.8	1801.7	1342.0	10,24
KIC 9414417	6253 ± 75	-0.13 ± 0.10	–	4.02 ± 0.03	1115.0 ± 32	60.1 ± 0.3	4.5 ± 1.1	1059.6	730.2	–	10
KIC 9592705	6174 ± 92	0.22 ± 0.10	–	3.97 ± 0.02	1008.0 ± 21	53.5 ± 0.3	4.9 ± 1.2	1265.4	971.0	728.3	10
KIC 9955598	5264 ± 95	0.08 ± 0.10	4.29 ± 0.12	4.48 ± 0.03	3546.0 ± 119	153.2 ± 0.1	9.0 ± 0.8	3606.2	2842.8	–	1,14,19
KIC 10514430	5784 ± 98	-0.11 ± 0.11	–	4.07 ± 0.02	1303.0 ± 30	70.0 ± 1.0	5.9 ± 0.7	1388.2	1006.9	–	10
KIC 10666592	6350 ± 80	0.26 ± 0.08	4.07 ± 0.08	4.02 ± 0.10	1115.0 ± 110	59.2 ± 0.6	4.5 ± 1.0	1569.2	1182.2	796.5	10,21
KIC 10963065	6090 ± 70	-0.25 ± 0.06	4.31 ± 0.08	4.29 ± 0.03	2184.0 ± 62	103.2 ± 0.6	7.1 ± 0.9	2338.8	1817.5	–	1,5,9,19
KIC 11295426	5793 ± 74	0.12 ± 0.07	4.28 ± 0.06	4.27 ± 0.01	2154.0 ± 13	101.6 ± 0.1	5.6 ± 0.8	2212.0	1767.4	–	14,16,23
KIC 11401755	5911 ± 66	-0.20 ± 0.06	4.05 ± 0.01	4.06 ± 0.04	1250.0 ± 44	67.9 ± 1.2	5.2 ± 1.4	1371.0	1100.9	–	7,10
KIC 11807274	6225 ± 66	0.06 ± 0.08	4.13 ± 0.01	4.14 ± 0.04	1496.0 ± 56	75.7 ± 0.3	8.1 ± 1.3	1680.9	1334.7	928.6	8,14

Note. References: 1: Appourchaux et al. (2012); 2: Ballard et al. (2014); 3: Ballot et al. (2011); 4: Benomar et al. (2014); 5: Bruntt et al. (2012); 6: Campante et al. (2015); 7: Carter et al. (2012); 8: Chaplin et al. (2013); 9: Chaplin et al. (2014); 10: Davies et al. (2016); 11: Deheuvels et al. (2016); 12: Escobar et al. (2012); 13: Everett et al. (2013); 14: Huber et al. (2013); 15: Huber et al. (2014); 16: Gilliland et al. (2013); 17: Lebreton & Goupil (2014); 18: Marcy et al. (2014); 19: Metcalfe et al. (2014); 20: Molenda-Żakowicz et al. (2013); 21: Pál et al. (2008); 22: Rowe et al. (2014); 23: Santos et al. (2013); and 24: Van Eylen et al. (2014).

$Z = 0.0172$, age $t = 4.57$ Gyr, and the mixing length parameter ($\alpha = 2.175$) are used for the MESA evolution code.

We use ADIPLS package (Christensen-Dalsgaard 2008) in MESA module to compute adiabatic oscillation frequencies of interior models. We compute ν_{\max} from Brown et al. (1991) with the solar values ($\nu_{\max\odot} = 3050 \mu\text{Hz}$ and $T_{\text{eff}\odot} = 5777$ K). For determination of the reference frequencies, we apply method in Paper I. Near surface region, because of lower sound speed, stellar evolution codes are difficult to simulate. Therefore, surface correction is needed. In this study, we apply surface correction in ADIPLS package (Kjeldsen, Bedding & Christensen-Dalsgaard 2008).

3.2 Modelling strategy and χ^2 method

The input parameters for the MESA evolution code are M_{mod} , initial helium ($Y_{0\text{mod}}$) and heavy element ($Z_{0\text{mod}}$) abundances and α . Among these parameters, $Z_{0\text{mod}}$ is derived from the observed metallicity ($[M/H]_{\text{obs}}$) (see below). For the models with diffusion, however, Z computed from $[M/H]_{\text{obs}}$ is the metallicity at the surface. α is taken as the solar value. During the calibration procedure, we properly change M_{mod} and $Y_{0\text{mod}}$ in order to fit models to the asteroseismic and non-asteroseismic constraints. If the calibration is not successful, we slightly modify $Z_{0\text{mod}}$. For all of these stars, we have $T_{\text{eff,S}}$ from spectra and gravity (g_{sca}) from the

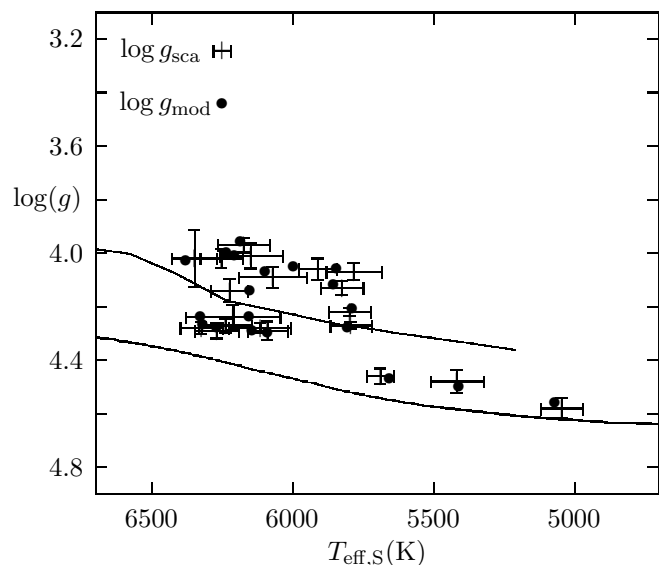


Figure 2. $\log g_{\text{sca}}$ for the 20 host stars is plotted with respect to $T_{\text{eff,S}}$ with their uncertainties. Also plotted is $\log g_{\text{mod}}$ with respect to T_{mod} of the best-fitting models (filled circles). Thin and thick solid lines are for the ZAMS and TAMS lines, respectively, taken from Yıldız (2015).

scaling relation as a function of $T_{\text{eff,S}}$ and ν_{max} :

$$\frac{g_{\text{sca}}}{g_{\odot}} = \frac{\nu_{\text{max}}}{\nu_{\text{max}\odot}} \left(\frac{T_{\text{eff,S}}}{T_{\odot}} \right)^{0.5}.$$

In Fig. 2, $\log g_{\text{sca}}$ is plotted with respect to $T_{\text{eff,S}}$. Also shown are the best-fitting models.

In fitting interior model of a star to the observational constraints, we first try to fit model of a star to the observed box in the $T_{\text{eff,S}} - \log g_{\text{sca}}$ diagram and secondly check how asteroseismic constraints are satisfied by oscillation frequencies of the model. The asteroseismic constraints comprise the observed oscillation frequencies, $\Delta\nu$, $\langle\delta\nu_{02}\rangle$, ν_{max} , and the reference frequencies ($\nu_{\text{min}0}$, $\nu_{\text{min}1}$, and $\nu_{\text{min}2}$). The best-fitting model is decided by applying χ^2 method (see below). We slightly change $\log g_{\text{mod}}$ and T_{mod} if needed for the minimization of χ^2 . For all of the host stars, except KIC 9955598, the difference between $T_{\text{eff,S}}$ and T_{mod} of the best-fitting model is less than 100 K.

The difference between $T_{\text{eff,S}}$ and T_{mod} of KIC 9955598 is 148 K. Effective temperatures of KIC 9955598 computed from its $B - V$ and $V - K$ colours are as 5355 and 5480 K, respectively. Its T_{mod} (5412 K) is very close to the mean (5418 K) of the $T_{\text{eff,S}}$ from the colours. In computation of its χ^2 , its observed T_{eff} is taken as 5418 K.

We compute normalized asteroseismic χ_{seis}^2 in order to evaluate resemblance rate between individual oscillation frequencies derived from observations and models:

$$\chi_{\text{seis}}^2 = \frac{1}{N_{\text{freq}}} \sum_{i=1}^{N_{\text{freq}}} \left(\frac{\nu_{\text{obs},i} - \nu_{\text{mod},i}}{\sigma_{\text{obs},i}} \right)^2, \quad (1)$$

where N_{freq} , $\nu_{\text{obs},i}$, and $\nu_{\text{mod},i}$ are number of observed oscillation frequencies, observed and model oscillation frequencies, respectively. $\sigma_{\text{obs},i}$ is uncertainty of the observed oscillation frequency.

To fit model oscillation frequencies to observed oscillation frequencies, density is the key parameter (see Paper III). However, different combinations of M and R may utilize the same mean density but completely different interior models for each of the M and R combinations. On account of this, we particularly pay attention to use the reference frequencies in our analysis. The reference frequencies strongly depend on M and R . Difference between the best model and observed reference frequencies for all of the host stars is in general less than $\Delta\nu/2$ (see Paper I).

The observed metallicity is included as input constraints on the models. Initial metallicity ($Z_{0\text{mod}}$) is computed from $[\text{M}/\text{H}]_{\text{obs}}$ given in Table 1 using with solar initial metallicity $Z_{0\odot}$: $Z_{0\text{mod}} = 10^{[\text{M}/\text{H}]_{\text{obs}}} Z_{0\odot}$. However, the mean uncertainty in $[\text{M}/\text{H}]_{\text{obs}}$ of the stars is about 0.11 dex. In addition, some extra difficulties in determination of $Z_{0\text{mod}}$ arise because of differentiation of surface metallicity from initial metallicity due to various processes such as diffusion and mixing. These processes strongly depend on stellar mass and the diffusion is in general not applicable for the stars with $M > 1.20 M_{\odot}$. Therefore, the metallicity is not involved in our non-seismic χ^2 analysis.

In computation of non-seismic χ^2 , we primarily focus on the observed effective temperature and surface gravity to fit model parameters:

$$\chi_{\text{spec}}^2 = \chi_{T_{\text{eff}}}^2 + \chi_{\log g}^2, \quad (2)$$

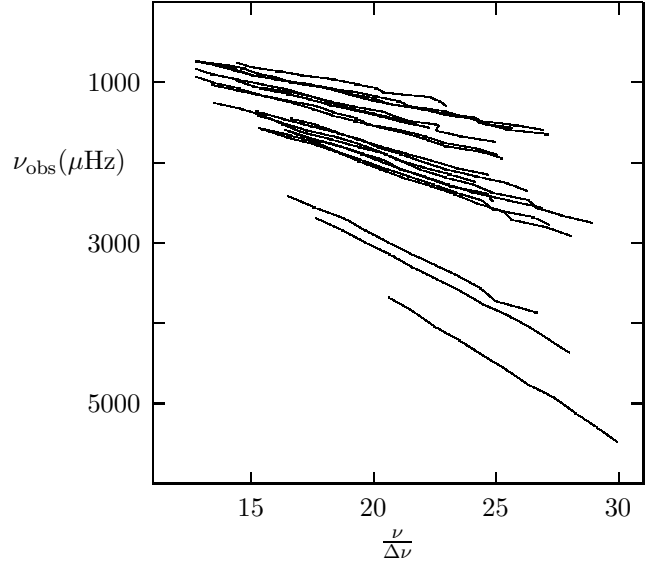


Figure 3. Observed oscillation frequencies (ν_{obs}) with $l = 0$ are plotted with respect to n'_{obs} for 20 planet and planet-candidate host stars. These lines show n'_{obs} of each host star. From high to low frequencies, stars evolve from MS to subgiant. KIC 3544595, KIC 9955598, and KIC 6278762 in the high-frequency region are located separately. The remaining stars are on the subgiant phase. They stand in the densest region. They have $700 < \nu_{\text{obs}} < 2900 \mu\text{Hz}$.

where

$$\chi_{T_{\text{eff}}}^2 = \left(\frac{T_{\text{eff,S}} - T_{\text{mod}}}{\sigma_{T_{\text{eff,S}}}} \right)^2, \quad (3)$$

where $\sigma_{T_{\text{eff,S}}}$ is uncertainty in $T_{\text{eff,S}}$. T_{mod} is effective temperature of the MESA model.

For asteroseismic and spectroscopic constraints, χ^2 is calculated independently in equation (1) and (2), respectively. For χ_{spec}^2 , uncertainties in $T_{\text{eff,S}}$ and $\log g$ are involved as in equation (2). $\chi_{\log g}^2$ is calculated from an equation similar to equation (3). χ_{spec}^2 of the host stars is listed in Table 2.

The difference between observed and model oscillation frequencies is in particular significant in the high-frequency domain. Therefore, we disregard some of the high-frequency data in computation of χ_{seis}^2 . This difference is due to the observational frequencies. As long as $\Delta\nu_{\text{obs}}$ is plotted with respect to $n'_{\text{obs}} = \frac{\nu_{\text{obs}}}{\Delta\nu_{\text{obs}}}$, the observed oscillation frequencies of the modes of some dwarfs with $n'_{\text{obs}} > 25$ are fluctuated. Uncertainties of the frequencies are significantly greater than that of the modes with $n'_{\text{obs}} < 25$ (see also fig. 3 in Paper III). Actually, this situation depends on evolutionary phase of a star. As it evolves from MS to the red giant branch (RGB), range of n'_{obs} is changed. In Fig. 3, observed oscillation frequencies with $l = 0$ are plotted with respect to n'_{obs} for 20 planet and planet-candidate host stars. However, observed oscillation frequencies of low-mass MS star, KIC 6278762, are in $21 < n'_{\text{obs}} < 30$ range. We notice the scattering of data of the modes with the two highest frequencies. Most of the stars is on the subgiant evolutionary phases, oscillation frequencies are observed in $13 < n'_{\text{obs}} < 27$ range.

Because of nuclear evolution during the MS phase, sound speed gradient changes inside the nuclear core.

Change in sound speed gradient causes $\delta\nu_{02}$ to decrease. This makes $\delta\nu_{02}$ a very suitable age indicator for the MS phase. The resolution is very high in a $\delta\nu_{02}$ - $\Delta\nu$ diagram for this phase (see e.g. White et al. 2011). Beyond the MS phase degeneracy sets in and it seems that $\delta\nu_{02}$ provides similar information as $\Delta\nu$.

As stated above, $\delta\nu_{02}$ is a very good age indicator for the MS stars. Therefore, observed value of $\delta\nu_{02}$ is used as one of the key constraints for the calibration of models of such stars. For all of the host stars, the difference between observed and model $\langle\delta\nu_{02}\rangle$ is less than $1 \mu\text{Hz}$, except KIC 5866724. For KIC 5866724, the difference is $1.1 \mu\text{Hz}$.

3.3 Results of the models

The results of interior model computations for the host stars are listed in Tables 2 and 3. According to these results, stellar mass range is 0.74 - $1.55 M_{\odot}$. KIC 10666592 and KIC 6278762 have the highest and the lowest masses, respectively. KIC 6278762 also has the lowest radius ($0.75 R_{\odot}$) and the oldest stellar age with 11.7 Gyr .

Most of the host stars have two reference minima in $\Delta\nu_{\text{obs}}$ versus ν_{obs} graph, especially $\nu_{\text{min}0}$ and $\nu_{\text{min}1}$. Besides these minima, KIC 3632418, KIC 8866102, KIC 9592705, KIC 10666592, and KIC 11807274 entirely or partly have min2. From the models, $\nu_{\text{min}2}$ is more stable than $\nu_{\text{min}0}$ and $\nu_{\text{min}1}$ for arbitrary mass and abundances. High-frequency region in $\Delta\nu$ versus ν graph is fluctuated. Therefore, $\nu_{\text{min}0}$ is either less or not confidential in some cases. Agreement between patterns of observed and model oscillation frequencies in $\Delta\nu$ versus ν graph reveals the appropriate model parameters.

In addition to KIC 9955598, we also computed T_{eff} and metallicity of four host stars (KIC 3632418, KIC 10963065, KIC 11295426, and KIC 11807274) from their colours using Lejeune, Cuisinier & Buser (1998) colour and bolometric correction (BC) tables. These results are in agreement with the spectroscopic results within the uncertainty in general.

We compare our derived fundamental parameters of the host stars with results obtained by Huber et al. (2013) and Silva Aguirre et al. (2015). In Huber et al. (2013), stellar parameters of 66 host stars from asteroseismic constraints are presented. Silva Aguirre et al. (2015) is determined stellar properties of 33 host stars using different grids of stellar evolutionary models. For $R_{\text{star}} < 1.3R_{\odot}$, the agreement between MESA and literature models of the host stars is excellent. However, significant discrepancy between MESA and literature radii occurs for the range $R_{\text{star}} > 1.3R_{\odot}$.

We also compare our results for stellar mass with the literature. Literature masses obtained from Huber et al. (2013) and Silva Aguirre et al. (2015) (M_{lit}) are plotted with respect to stellar mass derived from the MESA models (M_{mod}) in Fig. 5. There is mainly a very good agreement between M_{lit} and M_{mod} , especially for the masses lower than $1.1 M_{\odot}$. The significant difference appears for few stars.

3.4 Uncertainties in model parameters

The uncertainties in M_{mod} , R_{mod} , and age given in Table 2 are computed using the method obtained by Bellinger (2019). This method is a comprehensive method and developed for

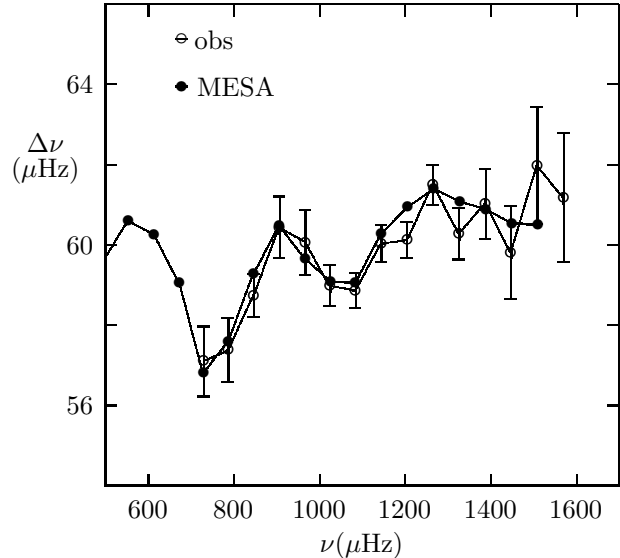


Figure 4. Comparison of MESA model (filled circle) and observed (circle) oscillation frequencies with $l = 0$ of KIC 9414417 in $\Delta\nu$ versus ν graph.

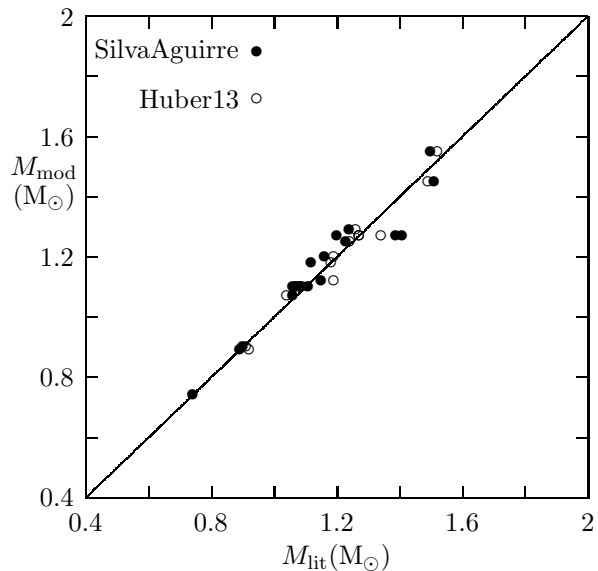


Figure 5. Stellar mass obtained by Huber et al. (2013) and Silva Aguirre et al. (2015) (M_{lit}) is plotted with respect to stellar mass derived from models (M_{mod}) in solar unit.

the MS and early subgiant stars. In this method, uncertainties of M_{mod} and R_{mod} are computed from uncertainties of T_{mod} , metallicity, $\langle\Delta\nu\rangle$, and ν_{max} . For the uncertainty in age, in addition to these parameters, $\langle\delta\nu_{02}\rangle$ is also included. Uncertainties of L_{mod} and $\log g_{\text{mod}}$ are derived from the uncertainties of M_{mod} , R_{mod} , and T_{mod} with a quadratic approach. For L_{mod} , for example,

$$\frac{\Delta L_{\text{mod}}}{L_{\text{mod}}} = \sqrt{\left(2 \frac{\Delta R_{\text{mod}}}{R_{\text{mod}}}\right)^2 + \left(4 \frac{\Delta T_{\text{mod}}}{T_{\text{mod}}}\right)^2}. \quad (4)$$

In the computations, ΔT_{mod} is taken the same as $\Delta T_{\text{eff,S}}$. All stars of the 20 hosts are either MS or early subgiant stars.

The uncertainty in $Y_{0\text{mod}}$ mostly depends on ΔM_{mod} be-

Table 2. Fundamental MESA model parameters of the host stars. M_{mod} , R_{mod} , T_{mod} , L_{mod} , $\log g_{\text{mod}}$, $Y_{0\text{mod}}$, $Z_{0\text{mod}}$, and t_{mod} are, respectively, stellar mass in M_{\odot} unit, stellar radius in R_{\odot} unit, effective temperature in K unit, luminosity in L_{\odot} unit, logarithm of surface gravity of the model in cgs, and age in units of Gyr. χ^2_{spec} of the models is in the last column.

Star	M_{mod} (M_{\odot})	R_{mod} (R_{\odot})	T_{mod} (K)	L_{mod} (L_{\odot})	$\log g_{\text{mod}}$ (cgs)	$Y_{0\text{mod}}$	$Z_{0\text{mod}}$	t_{mod} (Gyr)	χ^2_{spec}
HD 52265	1.23 ± 0.04	1.32 ± 0.01	6144 ± 110	2.24 ± 0.16	4.29 ± 0.04	0.274 ± 0.027	0.023 ± 0.002	3.1 ± 0.5	0.1
KIC 3544595	0.90 ± 0.10	0.92 ± 0.04	5658 ± 48	0.77 ± 0.07	4.47 ± 0.14	0.292 ± 0.097	0.015 ± 0.005	6.3 ± 2.2	2.7
KIC 3632418	1.27 ± 0.09	1.85 ± 0.05	6208 ± 111	4.55 ± 0.41	4.01 ± 0.09	0.283 ± 0.060	0.018 ± 0.004	3.9 ± 1.6	0.4
KIC 4349452	1.20 ± 0.05	1.31 ± 0.02	6270 ± 79	2.39 ± 0.14	4.28 ± 0.05	0.279 ± 0.035	0.017 ± 0.002	2.7 ± 0.9	0.0
KIC 5866724	1.27 ± 0.06	1.42 ± 0.02	6155 ± 167	2.61 ± 0.29	4.24 ± 0.06	0.274 ± 0.039	0.022 ± 0.003	2.9 ± 0.8	1.1
KIC 6278762	0.74 ± 0.03	0.75 ± 0.01	5072 ± 74	0.33 ± 0.02	4.56 ± 0.05	0.284 ± 0.035	0.012 ± 0.001	11.7 ± 2.7	0.6
KIC 6521045	1.10 ± 0.05	1.51 ± 0.03	5856 ± 75	2.41 ± 0.16	4.12 ± 0.06	0.277 ± 0.038	0.019 ± 0.003	7.3 ± 1.0	0.3
KIC 7296438	1.13 ± 0.04	1.39 ± 0.02	5790 ± 75	1.96 ± 0.12	4.20 ± 0.05	0.261 ± 0.028	0.023 ± 0.002	7.6 ± 0.7	0.5
KIC 8077137	1.18 ± 0.07	1.66 ± 0.04	6099 ± 121	3.43 ± 0.32	4.07 ± 0.08	0.279 ± 0.050	0.017 ± 0.003	5.2 ± 1.3	0.1
KIC 8292840	1.12 ± 0.05	1.33 ± 0.02	6328 ± 94	2.54 ± 0.17	4.24 ± 0.05	0.289 ± 0.039	0.012 ± 0.002	3.5 ± 0.7	1.0
KIC 8866102	1.25 ± 0.05	1.36 ± 0.02	6320 ± 75	2.66 ± 0.15	4.27 ± 0.05	0.278 ± 0.033	0.019 ± 0.002	2.3 ± 0.7	0.0
KIC 9414417	1.27 ± 0.05	1.86 ± 0.03	6236 ± 75	4.72 ± 0.27	4.00 ± 0.05	0.280 ± 0.033	0.016 ± 0.002	3.9 ± 1.7	0.1
KIC 9592705	1.45 ± 0.06	2.10 ± 0.03	6187 ± 92	5.80 ± 0.38	3.96 ± 0.05	0.270 ± 0.034	0.026 ± 0.003	3.3 ± 0.9	0.0
KIC 9955598	0.89 ± 0.04	0.88 ± 0.01	5412 ± 95	0.60 ± 0.04	4.50 ± 0.05	0.280 ± 0.038	0.017 ± 0.002	8.2 ± 2.2	3.1
KIC 10514430	1.07 ± 0.05	1.59 ± 0.03	5846 ± 98	2.66 ± 0.20	4.06 ± 0.06	0.280 ± 0.039	0.016 ± 0.002	7.5 ± 1.7	0.4
KIC 10666592	1.55 ± 0.15	1.99 ± 0.07	6381 ± 80	5.92 ± 0.51	4.03 ± 0.12	0.281 ± 0.082	0.025 ± 0.007	1.9 ± 0.5	0.4
KIC 10963065	1.10 ± 0.04	1.23 ± 0.02	6090 ± 70	1.88 ± 0.11	4.30 ± 0.05	0.272 ± 0.030	0.014 ± 0.002	4.0 ± 1.2	0.0
KIC 11295426	1.10 ± 0.03	1.25 ± 0.01	5807 ± 74	1.60 ± 0.09	4.28 ± 0.03	0.273 ± 0.022	0.024 ± 0.002	6.8 ± 1.3	0.0
KIC 11401755	1.10 ± 0.05	1.64 ± 0.04	5998 ± 66	3.12 ± 0.20	4.05 ± 0.07	0.283 ± 0.039	0.013 ± 0.002	5.9 ± 3.1	1.7
KIC 11807274	1.29 ± 0.06	1.60 ± 0.02	6154 ± 66	3.31 ± 0.16	4.14 ± 0.05	0.277 ± 0.039	0.020 ± 0.003	3.5 ± 0.7	2.2

Table 3. Asteroseismic parameters of MESA models for the host stars. $\langle\delta\nu_{02,\text{mod}}\rangle$, $\langle\Delta\nu_{\text{mod}}\rangle$, $\nu_{\text{max,mod}}$, $\nu_{\text{min0,mod}}$, $\nu_{\text{min1,mod}}$, and $\nu_{\text{min2,mod}}$ are, respectively, mean small and large separation between model oscillation frequencies, model frequency of maximum amplitude, reference frequencies of model in μHz units. $\nu_{\text{max,mod}}$ is computed from scaling relations with T_{mod} and $\log g_{\text{mod}}$. Typical uncertainties for the reference frequencies are $\langle\Delta\nu_{\text{mod}}\rangle/2$.

Star	$\langle\delta\nu_{02,\text{mod}}\rangle$ (μHz)	$\langle\Delta\nu_{\text{mod}}\rangle$ (μHz)	$\nu_{\text{max,mod}}$ (μHz)	$\nu_{\text{min0,mod}}$ (μHz)	$\nu_{\text{min1,mod}}$ (μHz)	$\nu_{\text{min2,mod}}$ (μHz)
HD 52265	7.5	98.8	2087.8	2398.0	1857.1	1340.9
KIC 3544595	8.8	146.5	3305.8	3286.7	2702.4	2034.0
KIC 3632418	4.5	60.9	1096.5	1473.3	1065.5	762.4
KIC 4349452	7.9	98.4	2040.9	2488.8	1884.5	1397.0
KIC 5866724	6.5	89.8	1855.8	2174.3	1633.6	1223.3
KIC 6278762	8.5	180.6	4305.2	4221.5	3324.0	2606.5
KIC 6521045	5.0	77.4	1461.5	1647.1	1259.7	894.3
KIC 7296438	5.2	89.1	1781.9	1950.9	1489.5	1094.7
KIC 8077137	4.9	69.4	1271.1	1594.6	1148.3	847.3
KIC 8292840	6.9	93.1	1856.3	2344.6	1742.8	1274.7
KIC 8866102	7.6	94.5	1964.9	2521.7	1830.8	1342.0
KIC 9414417	4.6	59.8	1074.2	1066.3	742.5	433.5
KIC 9592705	4.2	54.0	970.0	1298.6	963.7	670.4
KIC 9955598	8.1	154.1	3621.6	3609.3	2842.4	2228.4
KIC 10514430	5.2	70.4	1278.4	1385.5	1077.4	800.4
KIC 10666592	4.4	59.2	1132.5	1602.6	1183.6	829.3
KIC 10963065	7.4	103.4	2145.9	2394.4	1859.2	1376.9
KIC 11295426	5.2	101.8	2130.6	2238.6	1769.2	1364.8
KIC 11401755	5.0	68.0	1228.7	1371.9	1081.6	796.8
KIC 11807274	5.5	75.9	1483.5	1836.4	1336.7	1002.5

cause we consider $Y_{0\text{mod}}$ and ΔM_{mod} as variable in order to fit model to the observed luminosity. Using the numerical logarithmic derivatives of model luminosity with respect to ΔM_{mod} and $Y_{0\text{mod}}$, we obtain $\Delta Y_{\text{mod}}/Y_{\text{mod}} \approx 3\Delta M_{\text{mod}}/M_{\text{mod}}$. We apply a similar method for uncertainty in Z_{mod} .

4 MASS AND RADIUS ESTIMATION OF THE PLANETS AND PLANET CANDIDATES

Most of the planets are discovered by transit method. Besides the method, RV is an important tool for non-transiting planetary systems. Confirmed planets by these methods highly depend on fundamental parameters of host stars. Especially, accuracy of stellar radius and mass is crucial. We

obtain fundamental parameters of the hosts by constructing interior models. In this section, we compute basic properties of 34 planets and also four planet candidates using these stellar parameters. Then, fundamental orbital and structure parameters of the transiting planets and planet candidates are revised.

30 planets of the host stars are detected by transit method. We revise radius, semimajor axis, and inclination of these planets in this study. Radii of the planets are computed using estimated stellar radius (R_{mod}) and observed transit data from Rowe et al. (2015). Semimajor axis of the planets is estimated using M_{mod} . We also derive orbital inclination of the transiting planets. The orbital inclination is computed from equation (13) in Seager & Mallén-Ornelas (2003). In that equation, we use R_{mod} and semimajor axis and also impact parameter. The impact parameter is taken from Rowe et al. (2015).

Estimated transiting planetary radius, semimajor axis, and orbital inclination are listed in Table 4. Radius range of the planets is 0.35-16.50 R_{\oplus} . Orbital inclination of the planets is approximately 90° . Semimajor axis range of the planets is 0.04-0.35 au. According to values of the semimajor axis and radius, Kepler-2b is classified as hot Jupiter. We also derive fundamental parameters of the planet candidates. These parameters are also derived for transiting planet candidates and listed in Table 5. The planet-candidates radius range is 0.55-3.15 R_{\oplus} .

In Fig. 6, fractional difference between the transit and revised radii of the planets and planet candidates ($\Delta R_p/R_p$) is plotted with respect to orbital period (P_{orb}) in units of day. This figure shows that the maximum difference between estimated and transit radii is about 25 per cent for Kepler-444 system.

We estimate the planetary mass for only the planets detected by RV method. Among the planets we consider, only four of them (HD 52265b, Kepler-25d, Kepler-68d, and Kepler-93c) have RV data. Estimated stellar masses are used in equation (1) in Lebreton & Goupil (2014) to obtain the planetary mass. Orbital period, eccentricity, inclination of planetary orbit, and semi-amplitude are taken from the literature. If eccentricity is not available in the literature, we assume that the orbit is circular. For the systems with unknown orbital inclination, we present the minimum mass ($M \sin i$). The estimated mass is plotted with respect to planetary mass from RV data in Fig. 7. Mass range of the planets is 0.95-3 M_{Jup} . Kepler-25d and Kepler-93c have the lowest and the highest masses, respectively.

The estimated planetary mass of HD 52265b is 16 per cent greater than the mass from the literature. Masses of Kepler-25d and Kepler-93c are estimated as 0.29 and 2.98 M_{Jup} , respectively. Updated mass of the non-transiting planets are listed in Table 6.

5 CONCLUSIONS

Asteroseismology has recently detected oscillation frequencies of many host stars. In this study, interior models with MESA code for 20 planet and planet-candidate solar-like oscillating host stars are constructed under influence of these observational constraints. Mass, radius, initial helium abundance, and age of the host stars on the different evolution-

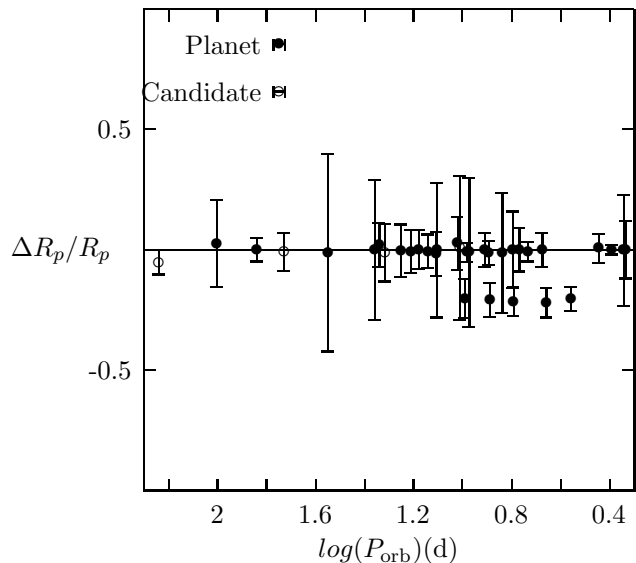


Figure 6. Fractional radius difference between transit and revised radius of the planets (filled circle) and planet candidates (circle) is plotted with respect to orbital period (P_{orb}) in days unit. $\Delta R_p/R_p$ is equal to $(R_{p,\text{transit}} - R_{p,\text{mod}})/R_{p,\text{mod}}$. Transit radius of the planet and planet candidates is taken from Rowe et al. (2015).

ary phases are derived from the constructed models. We also examine oscillation frequencies of these host stars observed by *CoRoT* and *Kepler*. Mean large and small separations between oscillation frequencies, and frequencies of the maximum amplitude are computed and used as constraints for the interior models. The reference frequencies also put very important constraints into interior models.

We find that model mass range of the host stars is 0.74-1.55 M_{\odot} . Among the host stars, KIC 6278762 and KIC 10666592 have the lowest (0.74 M_{\odot}) and highest masses (1.55 M_{\odot}), respectively. KIC 6278762 also has the lowest model radius (0.75 R_{\odot}) and is the oldest (11.7 Gyr) star among the host stars. Effective temperature and initial metallicity range of the host stars are 5000-6350 K and $Z_{0\text{mod}} = 0.012 - 0.026$, respectively.

Most of the host stars have two reference minima, especially $\nu_{\text{min}0}$ and $\nu_{\text{min}1}$, in $\Delta\nu_{\text{obs}}$ versus ν_{obs} graph. Besides these minima, KIC 3632418, KIC 8866102, KIC 9592705, KIC 10666592, and KIC 11807274 have either entire or part of the min2 glitch. From the models with arbitrary mass and abundance, we confirm that $\nu_{\text{min}2}$ is deeper than $\nu_{\text{min}0}$ and $\nu_{\text{min}1}$. min0 of the model oscillation frequencies is very shallow in comparison to min1. In addition, high-frequency region in $\Delta\nu$ versus ν graph for the observed oscillation frequencies is fluctuated. Therefore, $\nu_{\text{min}0}$ is either less or not confidential in some cases. Agreement between patterns of observed and model oscillation frequencies in $\Delta\nu$ versus ν graph, in particular for the range around $\nu_{\text{min}1}$ and $\nu_{\text{min}2}$, reveals the appropriate model parameters.

We also compute fundamental properties of 34 planets and also four planet candidates. Orbital and fundamental parameters of the transiting planets and planet candidates are revised. Radius range of the transiting planets is 0.35-16.50 R_{\oplus} . Orbital inclination of the planets is approximately 90° . Semimajor axis range of the planets is 0.04-0.35 au.

Table 4. Properties of the transiting planets. Planetary name, orbital period (P), radius [from the literature (R_{plit}) and this study (R_{p})], semimajor axis (a), and inclination (i) of the planetary orbit are presented. a and i are derived from this study. P and R_{plit} are taken from Rowe et al. (2015).

Planet	P (d)	R_{plit} (R_{\oplus})	R_{p} (R_{\oplus})	a (au)	i ($^{\circ}$)
Kepler-2b	2.204735 ± 0.000000	16.39 ± 0.15	16.42 ± 0.08	0.04 ± 0.01	90.00
Kepler-21b	2.785822 ± 0.000004	1.59 ± 0.01	1.58 ± 0.05	0.04 ± 0.01	84.95
Kepler-25b	12.720374 ± 0.000002	4.51 ± 0.08	4.52 ± 0.20	0.11 ± 0.01	89.66
Kepler-25c	6.238535 ± 0.000002	2.64 ± 0.04	2.64 ± 0.12	0.07 ± 0.01	89.95
Kepler-36b	16.231920 ± 0.000014	3.94 ± 0.05	3.97 ± 0.04	0.13 ± 0.01	87.61
Kepler-36c	13.849843 ± 0.000059	1.48 ± 0.02	1.49 ± 0.05	0.12 ± 0.01	89.18
Kepler-50b	7.812858 ± 0.000020	1.54 ± 0.03	1.56 ± 0.02	0.08 ± 0.01	88.27
Kepler-50c	9.376643 ± 0.000019	1.82 ± 0.03	1.84 ± 0.28	0.10 ± 0.01	87.34
Kepler-65b	5.859939 ± 0.000003	2.55 ± 0.04	2.55 ± 0.05	0.07 ± 0.01	89.84
Kepler-65c	2.154909 ± 0.000002	1.50 ± 0.03	1.50 ± 0.09	0.04 ± 0.01	83.02
Kepler-65d	8.131225 ± 0.000014	1.76 ± 0.03	1.76 ± 0.04	0.09 ± 0.01	86.15
Kepler-68b	5.398754 ± 0.000002	2.29 ± 0.03	2.31 ± 0.01	0.06 ± 0.01	89.89
Kepler-68c	9.605039 ± 0.000032	0.92 ± 0.01	0.93 ± 0.03	0.09 ± 0.01	89.74
Kepler-93b	4.726740 ± 0.000002	1.59 ± 0.04	1.59 ± 0.03	0.05 ± 0.01	86.88
Kepler-100b	12.815884 ± 0.000018	2.28 ± 0.06	2.32 ± 0.03	0.11 ± 0.01	87.85
Kepler-100c	6.887060 ± 0.000020	1.31 ± 0.03	1.33 ± 0.22	0.07 ± 0.01	87.19
Kepler-100d	35.333087 ± 0.000216	1.50 ± 0.03	1.52 ± 0.38	0.22 ± 0.01	88.91
Kepler-126b	10.495678 ± 0.000017	1.54 ± 0.02	1.50 ± 0.09	0.10 ± 0.01	87.50
Kepler-126c	100.282869 ± 0.000174	2.47 ± 0.04	2.41 ± 0.14	0.44 ± 0.06	89.98
Kepler-126d	21.869676 ± 0.000054	1.56 ± 0.03	1.53 ± 0.06	0.16 ± 0.02	88.40
Kepler-128b	15.089602 ± 0.000044	1.43 ± 0.03	1.43 ± 0.05	0.13 ± 0.01	89.93
Kepler-128c	22.802981 ± 0.000108	1.42 ± 0.03	1.42 ± 0.26	0.17 ± 0.01	88.30
Kepler-408b	2.465026 ± 0.000005	0.70 ± 0.01	0.70 ± 0.01	0.04 ± 0.01	85.89
Kepler-409b	68.958608 ± 0.000214	0.98 ± 0.02	0.98 ± 0.03	0.32 ± 0.01	89.90
Kepler-410Ab	17.833682 ± 0.000012	2.47 ± 0.04	2.48 ± 0.07	0.14 ± 0.01	90.00
Kepler-444b	3.600106 ± 0.000008	0.31 ± 0.03	0.39 ± 0.02	0.04 ± 0.01	88.27
Kepler-444c	4.545878 ± 0.000007	0.39 ± 0.04	0.50 ± 0.02	0.05 ± 0.01	88.60
Kepler-444d	6.189406 ± 0.000013	0.40 ± 0.04	0.51 ± 0.02	0.06 ± 0.01	89.13
Kepler-444e	7.743476 ± 0.000017	0.42 ± 0.04	0.53 ± 0.03	0.07 ± 0.01	88.99
Kepler-444f	9.740484 ± 0.000014	0.51 ± 0.05	0.64 ± 0.03	0.08 ± 0.01	89.75

Table 5. Properties of the transiting planet candidates. Columns are organized same as in Table 4.

Planet candidate	P (d)	R_{plit} (R_{\oplus})	R_{p} (R_{\oplus})	a (au)	i ($^{\circ}$)
KOI-263	20.719520 ± 0.000062	2.32 ± 0.05	2.35 ± 0.07	0.15 ± 0.01	89.92
KOI-288	10.275317 ± 0.000012	3.17 ± 0.06	3.15 ± 0.24	0.11 ± 0.01	87.06
KOI-364	173.877461 ± 0.000000	0.54 ± 0.03	0.57 ± 0.02	0.63 ± 0.03	89.93
KOI-974	53.505838 ± 0.000149	2.49 ± 0.06	2.51 ± 0.02	0.30 ± 0.02	89.98

Table 6. Properties of the non-transiting planets. Planetary name, orbital properties of the planets [period (P), semimajor axis (a), and eccentricity (e)], planetary mass [from the literature (M_{plit}) and this study (M_{p})] and references are presented. M_{spe} denotes the species of mass. P , a , e , and M_{spe} are taken from the literature.

Planet	P (d)	a (au)	e	M_{plit} (M_{jup})	M_{spe}	M_{p} (M_{jup})	Ref.
HD 52265b	119.60 ± 0.42	0.50 ± 0.35	0.03	1.05 ± 0.03	$M \sin i$	1.08 ± 0.03	Naef et al. (2001)
Kepler-25d	123.00 ± 2.00	–	–	0.28 ± 0.04	M	0.29 ± 0.05	Marcy et al. (2014)
Kepler-68d	580.00 ± 15.00	1.40 ± 0.03	0.18 ± 0.05	0.95 ± 0.04	$M \sin i$	0.96 ± 0.27	Gilliland et al. (2013)
Kepler-93c	1460.00	–	–	3.00	M	2.98	Marcy et al. (2014)

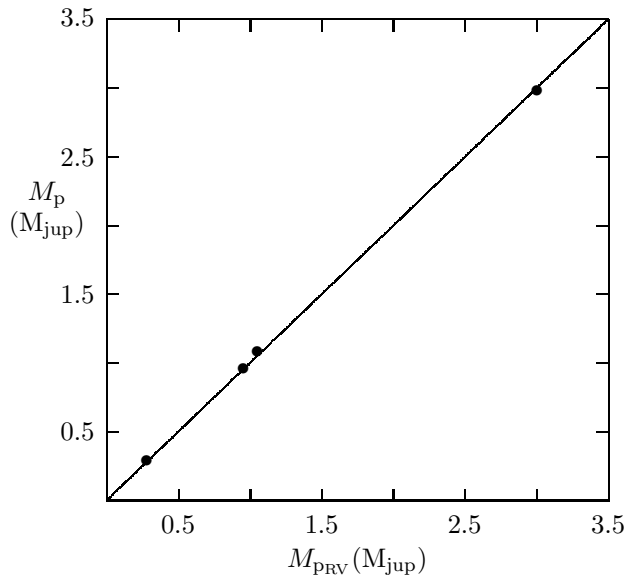


Figure 7. Estimated planetary mass is plotted with respect to mass from RV data in M_{jup} units.

According to the values of the semimajor axis and radius, Kepler-2b is classified as hot Jupiter. We also derive fundamental parameters of the planet candidates. Their radius range is $0.55\text{--}3.15 R_{\oplus}$. While the maximum difference between estimated and transit radii is about 25 per cent for the five planets in Kepler-444.

Mass range of the planets is $0.29\text{--}3 M_{\text{jup}}$. The estimated planetary mass of HD 52265b is 16 per cent higher than mass from the literature.

ACKNOWLEDGEMENTS

The anonymous referee is acknowledged for his/her suggestions which improved the presentation of the manuscript. We would like to thank Kelly Spencer for her kind help in checking the language of the revised manuscript.

REFERENCES

- Angulo C. et al., 1999, *Nucl. Phys. A*, 656, 3
 Appourchaux T. et al., 2012, *A&A*, 543, A54
 Baglin A., Michel E., Auvergne M., COROT Team, 2006, in Fletcher K., ed., *Proc. SOHO 18/GONG 2006/HELAS I (ESA SP-624)*, Beyond the Spherical Sun. ESA, Noordwijk, p. 34
 Ballard S. et al., 2014, *ApJ*, 790, 12
 Ballot J. et al., 2011, *A&A*, 530, A97
 Barclay T. et al., 2015, *ApJ*, 800, 46
 Bellinger E. P., 2019, *MNRAS*, 486, 4612
 Benomar, O., Masuda K., Shibahashi H., Suto Y., 2014, *PASJ*, 66, 94
 Böhm-Vitense E., 1958, *Zs. Ap.*, 46, 108
 Borucki W. et al., 2010, *Science*, 327, 977
 Brown T. M., Gilliland R. L., Noyes R. W., Ramsey L. W., 1991, *ApJ*, 368, 599
 Bruntt H. et al., 2012, *MNRAS*, 423, 122
 Campante T. L. et al., 2015, *ApJ*, 799, 170
 Carter J. A. et al., 2012, *Science*, 337, 556
 Chaplin W. J. et al., 2013, *ApJ*, 766, 101
 Chaplin W. J. et al., 2014, *ApJS*, 210, 1
 Christensen-Dalsgaard J., 2008, *Ap&SS*, 316, 113
 Cyburt R. H. et al., 2010, *ApJS*, 189, 240
 Davies G. R. et al., 2016, *MNRAS*, 456, 2183
 Deheuvels S., Brandão I., Silva Aguirre V., Ballot J., Michel E., Cunha M. S., Lebreton Y., Appourchaux T., 2016, *A&A*, 589, A93
 Escobar M. E. et al., 2012, *A&A*, 543, A96
 Everett M. E. et al., 2013, *ApJ*, 771, 107
 Gilliland R. L. et al., 2013, *ApJ*, 766, 40
 Huber D. et al., 2013, *ApJ*, 767, 127
 Huber D. et al., 2014, *ApJS*, 211, 2
 Iglesias C. A., Rogers, F. J., 1993, *ApJ*, 412, 752
 Iglesias C. A., Rogers, F. J., 1996, *ApJ*, 464, 943
 Kjeldsen H., Bedding T. R., 1995, *A&A*, 293, 87
 Kjeldsen H., Bedding T. R., Christensen-Dalsgaard J., 2008, *ApJ*, 683, L175
 Koch D. G. et al., 2010, *ApJL*, 713, L79
 Kunz R., Fey M., Jaeger M., Mayer A., Hammer J. W., Staudt G., Harissopulos S., Paradellis T., 2002, *ApJ*, 567, 643
 Lebreton Y., Goupil M. J., 2014, *A&A*, 569, A21
 Lejeune T., Cuisinier, F. Buser, R., 1998, *A&AS*, 130, 65
 Marcy G. W. et al., 2014, *ApJS*, 210, 20
 Mathur S. et al., 2012, *ApJ*, 749, 152
 Metcalfe T. S. et al., 2014, *ApJS*, 214, 27
 Molenda-Żakowicz J. et al., 2013, *MNRAS*, 434, 1422
 Naef D., Mayor M., Pepe F., Queloz D., Santos N. C., Udry S., Burnet M., 2001, *A&A*, 375, 205
 Narita N. et al., 2010, *PASJ*, 62, 779
 Nutzman P. et al., 2011, *ApJ*, 726, 3
 Pál A. et al., 2008, *ApJ*, 680, 1450
 Paxton B. et al., 2011, *ApJS*, 192, 39
 Paxton B. et al., 2013, *ApJS*, 208, 49
 Rowe J. F. et al., 2014, *ApJ*, 784, 45
 Rowe J. F. et al., 2015, *ApJS*, 217, 16
 Santos N. C. et al., 2013, *A&A*, 556, A150
 Seager S., Mallén-Ornelas G., 2003, *ApJ*, 585, 1038
 Silva Aguirre V. et al., 2015, *MNRAS*, 452, 2127
 Soriano M., Vauclair S., Vauclair G., Laymand M., 2007, *A&A*, 471, 885
 Steffen J. H. et al., 2012, *MNRAS*, 421, 2342
 Sullivan P. W. et al., 2015, *ApJ*, 809, 77
 Ulrich R. K., 1986, *ApJL*, 306, L37
 Van Eylen V. et al., 2014, *ApJ*, 782, 14
 White T. R. et al., 2011, *ApJL*, 742, L3
 Wright D. J. et al., 2011, *ApJ*, 728, L20
 Xie J-W., 2014, *ApJS*, 210, 25
 Yıldız M., 2015, *Res. Astron. Astrophys.*, 15, 2244
 Yıldız M., Çelik Orhan Z., Aksoy Ç., Ok S., 2014, *MNRAS*, 441, 2148 (Paper I)
 Yıldız M., Çelik Orhan Z., Kayhan C., 2015, *MNRAS*, 448, 3689 (Paper II)
 Yıldız M., Çelik Orhan Z., Kayhan C., 2016, *MNRAS*, 462, 1577 (Paper III)